HEFAT2010
7th International Conference on Heat Transfer, Fluid Mechanics and Thermodynmics
19-21 July 2010
Antalya, Turkey

REGULAR SURFACE PATTERNS ON RAYLEIGH-TAYLOR AND MARANGONI UNSTABLE EVAPORATING FILMS

Michael Bestehorn
Lehrstuhl für Theoretische Physik II, Brandenburgische Technische Universität,
Erich-Weinert-Strasse 1, 03046-Cottbus, Germany
E-mail: bes@physik.tu-cottbus.de

ABSTRACT

Thin volatile Newtonian liquid films with a free surface on the underside of a cooled horizontal substrate are studied theoretically and numerically. We show that if the fluid is initially in equilibrium with its own vapor in the gas phase below, regular surface patterns in the form of long-wave hexagons having a well defined lateral length scale are observed. This is in sharp contrast to the case without evaporation where rupture or coarsening to larger and larger patterns is seen in the long time limit. In this way, evaporation could be used for regular structuring of the film surface. The influence of a temperature dependent surface tension (Marangoni effect) is included as well, where special emphasis is layed on the so-called anomalous Marangoni effect. In this case a parameter region where stripes should occur is found by means of a weakly non-linear analysis.

INTRODUCTION

Surface patterns of thin liquid films on a solid support were studied during the last decade in numerous experimental and theoretical contributions (see [1, 2, 3, 4, 5, 6, 7, 8, 9] and references therein). In coating or wetting processes, a plane surface is usually desirable and the formation of surface deflections should be avoided. In contrast in modern (nano-) technological applications the creation and control of ordered structures come more and more into the focus of interest. Liquid thin films are applied in different ways to produce patterns with prescribed length scales and geometries. One possibility is to use a structured substrate [1, 2, 3]. In the present article we wish to concentrate on another method: the self-organized pattern growth due to an instability mechanism of the initially flat film [4, 5]. There are several mechanisms that may destabilize a flat surface and that allow to control the growth of surface patterns. Flat ultra-thin films may become unstable by van der Waals forces between surface and substrate [6, 7, 8].

NOMENCLATURE

d	[m]	thickness of liquid layer
d_g	[m]	thickness of gas layer
τ	[s]	vertical diffusion time of heat
κ	[m^2/s]	thermal diffusivity of liquid
ν	[m^2/s]	kinematic viscosity of liquid
ρ	[kg/m^3]	density of liquid
α	[W/mK]	thermal conductivity of liquid
α_g	[W/mK]	thermal conductivity of gas
Γ	[N/m]	surface tension
T	[K]	temperature
T_I	[K]	surface temperature
T_s	[K]	saturation temperature
T_0	[K]	reference temperature
T_u	[K]	temperature of substrate
J	[kg/m^2s]	mass flux density
P_s	[N/m^2]	saturation pressure
m	[kg]	molecular mass
Dimensionless quantities		
x, y, t		spatial coordinates, time
$h(x, y, t)$		thickness of liquid layer
h_0		equilibrium thickness
λ		linear growth rate
$\vec{k}$		2D wave vector
$\vec{x}$		2D horizontal vector
M		Marangoni number
B		Biot number
G		gravity number
C		Crispation number
E		Evaporation number
$\tilde{\alpha}$		accommodation coefficient
$\xi_k(t)$		Fourier mode amplitudes
$c^{(2)}_{kk'k''}$, $c^{(3)}_{kk'k''k'''}$		non-linear expansion coefficients
$\xi_1, \xi_2, \xi_3, \xi_4$		order parameters
ξ_s		amplitudes of slaved modes
ϵ		bifurcation parameter
A, c_i		Landau coefficients
k_c		critical wave number
Constants		
g	9.81 m/s^2	gravitational acceleration
k	1.38·10^{-23} J/K	Boltzmann's constant

Thicker films can be destabilized by inhomogeneous tangential surface tensions, which in turn are often caused by lateral gradients of temperature and/or, in mixtures, of concentration [9, 10, 11, 12, 13].

A rather simple method for destabilization is to put the film upside down, i.e. to position it under a flat horizontal plate. Then gravity acts against the stabilizing surface tension and inhomogeneous surface patterns result [14]. This is called Rayleigh-Taylor instability (RTI) (Figs.1,2).

In the present paper, we shall first concentrate on the Rayleigh-Taylor instability as destabilizing mechanism of the flat surface. In addition we assume a vertical heat gradient applied from outside. Further we neglect convective heat transfer in both layers. If the fluid is heated from below (from the gas side), this usually would stabilize the flat film. As was shown in [14], RTI may occur if the temperature gradient is not too large and film rupture is avoided by the stabilizing Marangoni effect.

In previous works, evaporation was considered as a destabilizing mechanism. Here we shall concentrate on the opposite case. Assume that the fluid is heated from below (or cooled from above). If the partial pressure of the vapor in the gas layer under the fluid is equal to the saturation pressure belonging to the surface temperature of the initial flat film, then a small elevation of the surface into colder regions leads to local condensation, a small depression into hotter regions causes evaporation.

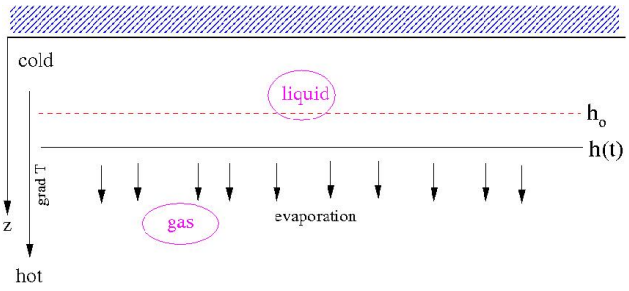

Figure 1 The flat surface of a fluid under a horizontal plate heated from below is stable at position h_0 where liquid and gas layers are in thermodynamic equilibrium. If the surface is at position h the liquid would evaporate, if it would be below h_0 it would condensate until h_0 is reached.

In a previous publication [15] we showed that this mechanism may avoid rupture for large enough evaporation rates even without the Marangoni effect. Moreover, due to the modified character of the instability, coarsening does no longer occur in the long time limit. Instead we found very regular cell structures in the form of hexagons, known from their morphology from small scale convection in thicker fluid layers [16, 17, 18].

THIN FILM EQUATION AND EVAPORATION

Up to now, most of the theoretical work is based on an interface equation, often called thin film equation, describing the location $z = h(x, y, t)$ of the free surface of the liquid [4, 19, 20, 21]. This equation can be systematically derived from the Navier-Stokes equation using the lubrication approximation and reads:

$$\partial_t h = -\nabla \left[-\frac{1}{2}\frac{MBh^2}{(1+Bh)^2}\nabla h + \frac{1}{3}h^3 C^{-1}\Delta\nabla h + \frac{1}{3}Gh^3\nabla h \right] , \tag{1}$$

where ∇ and Δ denote the horizontal gradient and Laplace operators. In (1) a scaling for lengths and time according to

$$(x, y, z, h) = (\tilde{x}, \tilde{y}, \tilde{z}, \tilde{h}) \cdot d, \quad t = \tilde{t} \cdot \tau, \quad \tau = d^2/\kappa$$

is used (tilde means dimensionless, omitted in (1)). The thickness of the fluid layer is d, τ denotes the vertical diffusion time of heat, and κ is the thermal diffusivity of the liquid. Scaling results into the dimensionless numbers M (Marangoni number), B (Biot number), G (gravity number), C (Crispation number) defined as

$$M = \frac{\gamma_T \Delta T d}{\rho\nu\kappa}, \quad B = \frac{\alpha_g d}{\alpha d_g}, \quad G = \frac{g d^3}{\nu\kappa}, \quad C = \frac{\gamma_0 d}{\kappa\nu\rho} .$$

Here, surface tension is assumed to be a linear function of surface temperature T_I

$$\Gamma = \gamma_0 - \gamma_T (T_I - T_0) , \qquad \gamma_0, \gamma_T > 0 . \tag{2}$$

Viscosity, density, and thermal conductivity of the fluid are denoted with ν, ρ, and α. The width of the gas layer is d_g, α_g is its thermal conductivity and g the gravitational acceleration.

Previous work shows that in the case of a surface-driven thermal instability, rupture of the film occurs after a relatively short time [12, 22, 23]. Rupture means that the surface function h reaches zero. From that moment on the thin film equation is meaningless since points occur where h is no longer differentiable. To avoid rupture, a repelling short range interaction can be introduced. Then patterns in the long time limit may be studied and show coarsening, a slow increase of the lateral dimensions of the structures (drops or holes) until one big hole (or drop) eventually remains [13, 24].

Evaporation and condensation

Additional effects caused by (moderate) evaporation or condensation on the interface can be included easily in the formalism [25, 26]. A term of the form J/ρ has to be added on the r.h.s. of eq.(1), where J denotes the mass flux density. In general, J is a complicated function of temperature, pressure, and fluid parameters. It can be roughly estimated using a Hertz-Knudsen law:

$$J(T, P_e) = \alpha \cdot (P_s(T) - P_v) \cdot \sqrt{\frac{m}{2\pi k T}} \tag{3}$$

where P_s is the saturation pressure of the liquid, P_v the partial pressure of vapor in the atmosphere below the film,

m the molecular mass of the fluid particles and k Boltzmann's constant. The so-called accommodation coefficient α accounts for an adjustment of the real conditions at the surface on the idealized assumptions used for deriving the Hertz-Knudsen law. It must be less then one but, depending on the experimental situation, can be as small as $10^{-3}..10^{-6}$.

Assuming a linear temperature profile in vertical direction inside the liquid and a vanishing mass flux at equilibrium height h_0, eq.(3) can be expanded with respect to $h - h_0$. In the same scaling used for eq.(1), the additional term to eq. (1) now reads (for details see [15])

$$-E\,(h - h_0)\;, \tag{4}$$

where E is the dimensionless evaporation number

$$E = \frac{\tilde{\alpha}\tau}{\rho} \cdot \frac{T_I - T_u}{d}\;.$$

Here, T_I is the temperature of the free surface, T_u that of the solid plate. For $\tilde{\alpha}$ one finds

$$\tilde{\alpha} = \alpha \cdot (m/2\pi k T_s)^{1/2} (dP_s/dT)_{T_s}$$

where T_S is the saturation temperature at P_s. For water with T_s at room temperature one finally has

$$\tilde{\alpha} \approx \alpha \cdot 0.13\mathrm{Kg}/(\mathrm{m^2 s\ K})$$

Stability of the flat film, Turing structures

Performing a standard linear stability analysis for the flat film at equilibrium thickness of the form

$$h(\vec{x}, t) = h_0 + \eta \exp(\lambda t + i\vec{k}\vec{x})\;,$$

one finds for the growth rate λ

$$\lambda(k^2) = \left[-\frac{1}{2}\frac{MBh_0^2}{(1+Bh_0)^2} + \frac{1}{3}Gh_0^3\right] k^2 - \frac{1}{3}C^{-1}h_0^3 k^4 - E\;.$$

As long as $E > 0$ ($T_I > T_u$, heated from below) it has the typical shape of a Turing instability (fig.2) or type I instability [27].

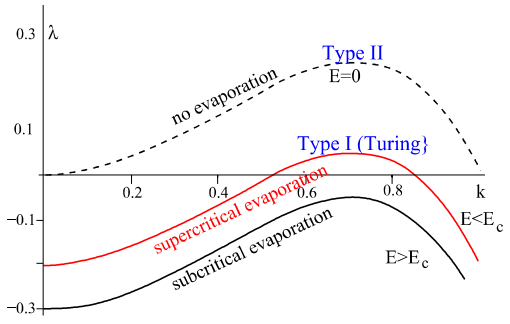

Figure 2 Growth rates over wave number for several values of E. Without evaporation, the instability is of type II [27].

If the evaporation rate remains below a critical value E_c, a whole band of wave vectors localized around a final critical one k_c may linearly grow and show spatially periodic patterns, as discussed in the following section (fig.3).

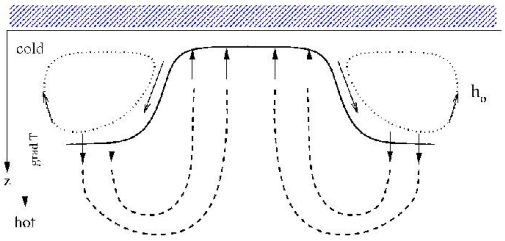

Figure 3 Sketch of a stationary Turing instability. If the surface is deflected around the value h_0 thicker parts evaporate, thinner regions condensate. This stabilizing mechanism may be overcome by gravitation and a Type I instability may occur.

NON-LINEAR PATTERN FORMATION

2D Control parameter plane

Eq. (1) with (4) includes 5 independent control parameters. To reduce this to three, a secondary scaling according to

$$h = \sqrt{M/G}\;\tilde{h}, \quad x = (GC)^{-1/2}\;\tilde{x}, \quad t = G^{-1/2}M^{-3/2}C^{-1}\;\tilde{t}$$

is in order. This yields the three new (combined) control parameters

$$\begin{aligned} \tilde{h}_0 &= h_0 \cdot \sqrt{G/M},\ \tilde{B} = B \cdot (M/G)^{1/2}, \\ \tilde{E} &= E \cdot C^{-1} G^{-1/2} M^{-3/2}\;. \end{aligned}$$

The scaled equation we use further thus reads

$$\begin{aligned} \partial_{\tilde{t}}\tilde{h} &= -\tilde{\nabla}\left[-\frac{1}{2}\frac{\tilde{B}\tilde{h}^2}{(1+\tilde{B}\tilde{h})^2}\tilde{\nabla}\tilde{h} + \frac{1}{3}\tilde{h}^3\tilde{\Delta}\tilde{\nabla}\tilde{h} + \frac{1}{3}\tilde{h}^3\tilde{\nabla}\tilde{h}\right] \\ &\quad -\tilde{E}\cdot(\tilde{h} - \tilde{h}_0) \end{aligned} \tag{5}$$

Fig.4 shows the $\tilde{E} - \tilde{h}_0$ plane. Inside the shaded area, which is limited by

$$\tilde{E}_{\max} = \tilde{h}_0^3/12 \tag{6}$$

$$\tilde{E}_{\min} = \frac{3}{256\tilde{h}_0} - \frac{\tilde{h}_0}{16} + \frac{\tilde{h}_0^3}{12}, \quad \tilde{h}_0 > \sqrt{3/8}, \tag{7}$$

$\tilde{B}$ can always be chosen in such a way, that an instability occurs via Turing type. Left of the shaded area, the flat film remains stable, on its right hand side, it is always unstable and no critical point exists.

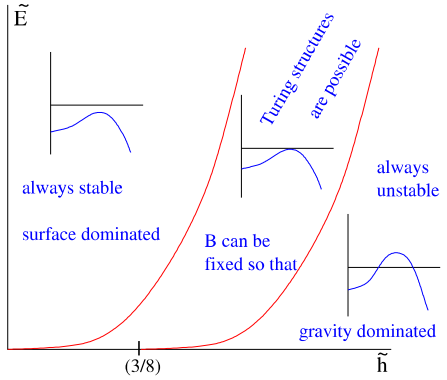

Figure 4 Control parameter plane for eq. (5). Inside the shaded area, interesting pattern forming instabilities of Turing type are expected.

Numerical solutions

To show what happens in the non-linear regime, we perform a direct numerical simulation of (5) in two spatial dimensions with periodic boundary conditions. As initial condition, a random dot distribution around h_0 is used. The method is based on a pseudo-spectral scheme developed earlier and used for the thin film equation without evaporation, for details see [13].

To demonstrate the qualitative influence of evaporation on pattern formation, we start with a run without evaporation ($E = 0$, top row of fig.5). Rupture occurs soon after almost the whole mass of the liquid film is condensed in a single spot (see arrows in fig.5) somewhere in the middle of the layer. For $E > 0$ the scenario is completely different (bottom row). After an initial phase, large scale hexagons occur and are finally found to be stable.

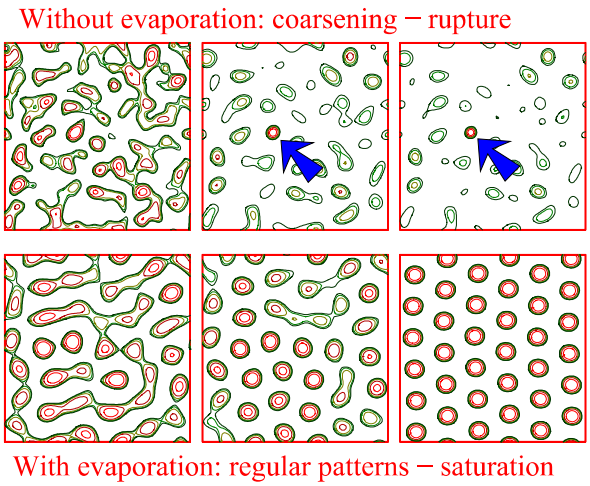

Figure 5 Two time series as numerical solutions of (5). Without evaporation rupture occurs soon, with evaporation, a typical regular pattern of hexagons emerges.

Numerically, we tried other values inside the shaded region of fig.4. For all values, hexagons resembling those of fig.5. were found with a size corresponding roughly to the critical wave number that maximizes the growth rate (see fig.2).

THE WEAKLY NON-LINEAR REGIME

To shed light on pattern formation and selection above but still close to instability, it is instructive to study the weakly non-linear regime. To this end we first go to Fourier space writing (in the following we drop the tildes over the arguments)

$$\tilde{h}(\vec{x},t) = \tilde{h}_0 + \sum_k \xi_k(t) \mathrm{e}^{i\vec{k}\vec{x}}, \qquad \xi_k = \xi^*_{-k} \ .$$

Inserting this into (5) and expanding the non-linearities up to the third order in the amplitudes ξ_k yields a set of ODEs

$$d_t\xi_k = \lambda(k)\xi_k + \sum_{k'k''} c^{(2)}_{kk'k''}\xi_{k'}\xi_{k''} + \sum_{k'k''k'''} c^{(3)}_{kk'k''k'''}\xi_{k'}\xi_{k''}\xi_{k'''} \tag{8}$$

with

$$\lambda(k) = \left[-\frac{1}{2}\frac{\tilde{B}\tilde{h}_0^2}{(1+\tilde{B}\tilde{h}_0)^2} + \frac{1}{3}\tilde{h}_0^3\right] k^2 - \frac{1}{3}\tilde{h}_0^3 k^4 - \tilde{E} \ .$$

Order parameter equations

Now we may distinguish between amplitudes belonging to k-values where $\lambda(k) > 0$, called active modes or *order parameters*, and those where λ is negative. The latter are the passive or *slaved modes* (denoted by the index s) and may be found from (8) by adiabatic elimination [28]. In lowest (2nd) order of the order parameters they read

$$\xi_s \approx -\frac{1}{\lambda_s}\sum_{ij} c^{(2)}_{sij}\xi_i\xi_j \ , \tag{9}$$

where the sums run only over the order parameters. Eliminating the slaved modes from (8) by the help of (9) gives a closed set of equations only for the order parameters. If we want to find out if stripes, squares or hexagons are stable above threshold, it is sufficient to take only four order parameters with wave vectors sketched in fig.6.

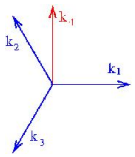

Figure 6 Orientation of the $\vec{k}$-vectors for the order parameters of (10). All vectors lay on a circle with $|\vec{k}| = k_c$.

Then the order parameter equations read

$$\begin{aligned}
d_t\xi_1 &= \epsilon\,\xi_1 + A\,\xi_2^*\xi_3^* + \xi_1\left(c_1|\xi_1|^2 + c_2|\xi_2|^2 + c_3|\xi_3|^2 + c_4|\xi_4|^2\right)\\
d_t\xi_2 &= \epsilon\,\xi_2 + A\,\xi_1^*\xi_3^* + \xi_2\left(c_1|\xi_2|^2 + c_2|\xi_1|^2 + c_3|\xi_3|^2 + c_4|\xi_4|^2\right)\\
d_t\xi_3 &= \epsilon\,\xi_3 + A\,\xi_1^*\xi_2^* + \xi_3\left(c_1|\xi_3|^2 + c_2|\xi_1|^2 + c_3|\xi_2|^2 + c_4|\xi_4|^2\right)\\
d_t\xi_4 &= \epsilon\,\xi_4 + \xi_4\left(c_4|\xi_1|^2 + c_2'|\xi_2|^2 + c_3'|\xi_3|^2 + c_1|\xi_4|^2\right)
\end{aligned} \tag{10}$$

with $\epsilon = \lambda(k_c^2)$ as (small) distance from threshold. The non-linear coefficients (Landau coefficients) are found as

$$\begin{aligned} A &= k_c^2\left(\frac{\tilde{B}\tilde{h}_0}{(1+\tilde{B}\tilde{h}_0)^3}+\tilde{h}_0^2(1-k_c^2)\right) \\ c_1 &= C-\frac{2}{\lambda(2k_1)}A\left(A-6\tilde{h}_0^2k_c^4\right) \\ c_2=c_3 &= 2C-\frac{3}{\lambda(k_1-k_2)}A\left(A-3\tilde{h}_0^2k_c^4\right) \\ c_4 &= 2C-\frac{4}{\lambda(k_1-k_4)}A\left(A-\tilde{h}_0^2k_c^4\right) \end{aligned}$$

with

$$C=k_c^2\left(\frac{1}{2}\frac{\tilde{B}(1-2\tilde{B}\tilde{h}_0)}{(1+\tilde{B}\tilde{h}_0)^4}+\tilde{h}_0(1-k_c^2)\right)$$

and the wave vector of the linearly fastest growing mode is

$$k_c^2=\sqrt{3\tilde{E}/\tilde{h}_0^3}\ .$$

Stability beyond threshold

There are four topologically different stationary solutions of (10):
(i) stripes with

$$\xi_1=\sqrt{-\epsilon/c_1},\qquad \xi_2=\xi_3=\xi_4=0\ ,$$

(ii) squares with

$$\xi_1=\xi_4=\sqrt{-\epsilon/(c_1+c_4)},\qquad \xi_2=\xi_3=0\ ,$$

(iii,iv) up and down hexagons

$$\xi_1=\xi_2=\xi_3=\frac{-A\pm\sqrt{A^2-4\epsilon(c_1+c_2+c_3)}}{2(c_1+c_2+c_3)},\quad \xi_4=0\ .$$

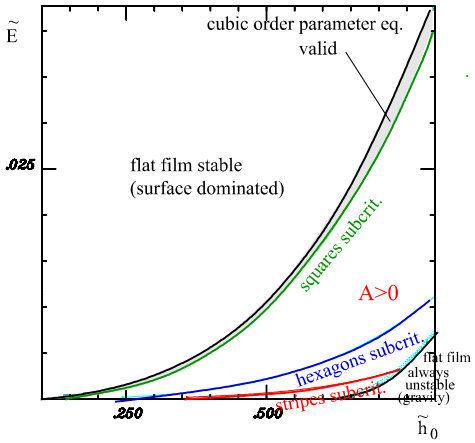

Figure 7 Stability diagram based on order parameter eqs. In the Turing pattern regime, the cubic equations are valid only in the tiny shaded region.

Each of these solutions exists only for Landau coefficients giving a real valued root for the corresponding amplitudes.

However, computing the coefficients it turns out that the validity of the cubic order parameter eqs. is rather limited. Only in the shaded area of fig.7, all roots are found to be real valued. In almost the whole area, squares are subcritical ($c_1+c_4>0$) and one should go up to the 5th order to say something on their stability. At least one may detect that the quadratic coefficient A is always positive and therefore one may expect up-hexagons (if no 5th-order squares would be more stable).

Anomalous Marangoni effect

There are several aqueous alcohol solutions where surface tension increases with increasing temperature for a certain working temperature [29]. This behavior is called *anomalous Marangoni effect* and covered by (2) if $\gamma_T<0$. If such a fluid is heated from the gas side, the Marangoni effect becomes destabilizing. If we put our system upside down, gravity acts now stabilizing. Such a fluid layer is also described by eq. (1), one has just to substitute M by $-M$ and G by $-G$. The scaled version (5) thus reads

$$\begin{aligned} \partial_{\tilde{t}}\tilde{h} &= -\tilde{\nabla}\left[\frac{1}{2}\frac{\tilde{B}\tilde{h}^2}{(1+\tilde{B}\tilde{h})^2}\tilde{\nabla}\tilde{h}+\frac{1}{3}\tilde{h}^3\tilde{\Delta}\tilde{\nabla}\tilde{h}-\frac{1}{3}\tilde{h}^3\tilde{\nabla}\tilde{h}\right] \\ &\quad -\tilde{E}\cdot(\tilde{h}-\tilde{h}_0)\ . \end{aligned} \tag{11}$$

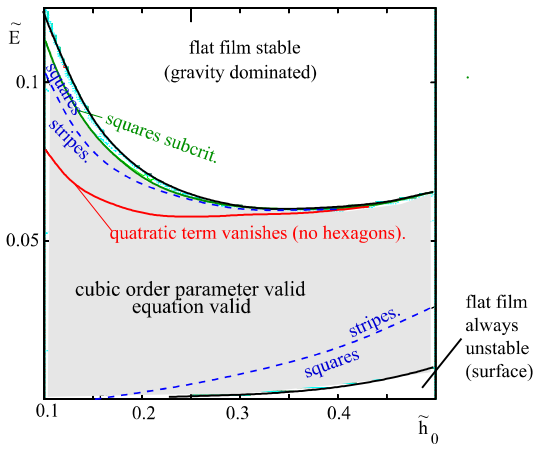

Figure 8 Stability diagram of the anomalous Marangoni effect. The order parameter eqs. now cover almost the complete Turing region. Depending on parameters, up,down hexagons or squares can be stable.

The shape of the region in the $\tilde{E}-\tilde{h}_0$ plane where Turing patterns occur (fig.4) is now changed and limited by

$$\tilde{E}_{\max} = \frac{3}{256\tilde{h}_0}+\frac{\tilde{h}_0}{16}+\frac{\tilde{h}_0^3}{12} \tag{12}$$

$$\tilde{E}_{\min} = \tilde{h}_0^3/12\ . \tag{13}$$

Note that $\tilde{E}_{\max}$ goes to infinity if $\tilde{h}_0 \to 0$. The reason is that for very thin layers the destabilizing Marangoni effect becomes more and more important and stabilizing gravity can then be neglected.

Repeating the weakly non-linear analysis shows now that the cubic order parameter eqs. are valid in almost the whole region of interest (fig.8). It is remarkable that the quadratic coefficient A may change sign along a codimension-one line. Near this line, stripes should occur as a first bifurcation. Stripes bifurcate forward, hexagons backwards. The subcritical range for hexagons is given by

$$\epsilon > \frac{A^2}{4(c_1 + c_2 + c_3)} \ .$$

Fig. 9 shows a time series found by a numerical solution of (11) for parameters where $A \approx 0$. As expected from the order parameter eqs., hexagons are not stabilized and stripes are the selected planform.

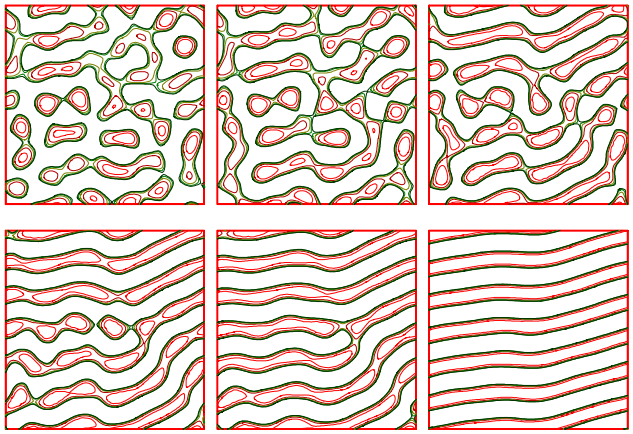

Figure 9 Numerical solution of (11) for parameters where $A \approx 0$. Stripes are the preferred structure.

CONCLUSIONS

We showed that evaporation may stabilize a flat liquid film surface if the layer is heated from the gas side. If instability sets in, the typical scenario characteristic for thin films without evaporation is completely changed. Instead of coarsening and rupture one finds Turing like patterns, hexagons for normal fluids and stripes or hexagons if the Marangoni effect is anomalous, as in certain long-chain-alcohol solutions. These results were obtained both from a weakly non-linear analysis as well as from direct numerical simulations of the thin-film equation.

Finally it is important to note that the hexagons found in our study are still on a large scale compared to the layer depth. Although looking similar to the classical small scale structures obtained in Bénard-Marangoni convection, the behavior of the thin film fluid is completely different. Deformation plays a crucial role, whereas for small scale structures the surface can assumed to be flat in a good approximation.

References

[1] N. Rehse et al., Eur. Phys. J. **E4**, 69 (2001).

[2] L. Rockford et al., Phys. Rev. Lett. **82**, 2602 (1999).

[3] R. Borcia, M. Bestehorn, Langmuir **25**, 1919 (2009)

[4] A. Oron, S. H. Davis, S. G. Bankhoff, Rev. Mod. Phys. **69**, 931 (1997).

[5] A. Pototsky, M. Bestehorn, U. Thiele, Physica **D199**, 138 (2004).

[6] G. Reiter et al., Langmuir **15**, 2551 (1999).

[7] G. Reiter, Phys. Rev. Lett. **68**, 75 (1992).

[8] K. Jacobs, S. Herminghaus, K. R. Mecke, Langmuir **14**, 965 (1998).

[9] P. Colinet, J. C. Legros, M. G. Velarde, *Nonlinear Dynamics of Surface-Tension-Driven Instabilities*, Wiley-VCH Berlin (2001).

[10] J. P. Burelbach, S. G. Bankoff, S. H. Davis, J. Fluid Mech. **195**, 463 (1988).

[11] J. P. Burelbach, S. G. Bankoff, S. H. Davis, Pys. Fluids **A2**, 322 (1990).

[12] A. Oron, Phys. Fluids **12**, 1633 (2000).

[13] M. Bestehorn, A. Pototsky, U. Thiele, Eur. Phys. J. B **33**, 457 (2003).

[14] R. J. Deissler, A. Oron, Phys. Rev. Lett. **68**, 2948 (1992).

[15] M.Bestehorn, D.Merkt, Phys. Rev. Lett. **97**, 127802 (2006)

[16] M. Bestehorn, Phys. Rev. **E48**, 3622 (1993).

[17] K. Eckert, M. Bestehorn, A. Thess, J. Fluid Mech. **356**, 155 (1998).

[18] D. Semwogerere, M. F. Schatz, Phys. Rev. Lett. **88**, 054501 (2002).

[19] A. Vrij, Discuss. Faraday Soc. **42**, 23 (1966).

[20] L. M. Pismen, Y. Pomeau, Phys. Rev. E **62**, 2480 (2000)

[21] M. Bestehorn, K. Neuffer, Phys. Rev. Lett. **87**, 046101 (2001).

[22] A. A. Golovin, A. A. Nepomnyashchy, L. M. Pismen, J. Fluid Mech. **341**, 317 (1997).

[23] M. J. Tan, S. G. Bankoff, S. H. Davis, Pys. Fluids **A2**, 313 (1990).

[24] M.Bestehorn, *Fluid Dynamics and Pattern Formation*, Contribution to *Encyclopedia of Complexity and System Science*, Ed. R.A.Meyers, Springer Berlin (2009)

[25] A. V. Lyushnin, A. A. Golovin, L. M. Pismen, Phys. Rev. **E65**, 021602 (2002).

[26] A. Oron, Phys. Rev. Lett. **85**, 2108 (2000).

[27] M.C. Cross, P.C. Hohenberg, Rev. Mod. Phys. **65**, 851 (1993)

[28] H. Haken, *Synergetics: Introduction and Advanced Topics*, Springer Berlin, 3rd ed. (2004)

[29] J.C. Legros, G. Petre, M.C. Limbourg-Fontaine, Adv. Space Res. **4**, 37 (1984)